Coupling effects on the fusion of ^{6}Li + ^{154}Sm at energies slightly above the Coulomb barrier

C. L. Guo,[1] G. L. Zhang,[1,*] S. P. Hu,[2,3] J. C. Yang,[1] H. Q. Zhang,[2,†] P. R. S. Gomes,[4] J. Lubian,[4] X. G. Wu,[2] J. Zhong,[2,3] C. Y. He,[2] Y. Zheng,[2] C. B. Li,[2] G. S. Li,[2] W. W. Qu,[1] F. Wang,[1] L. Zheng,[1] L. Yu,[1] Q. M. Chen,[2] P. W. Luo,[2,3] H. W. Li,[2,5] Y. H. Wu,[2,5] W. K. Zhou,[2] B. J. Zhu,[2] and H. B. Sun[3]

[1]*School of Physics and Nuclear Energy Engineering, Beihang University, Beijing 100191, China*

[2]*China Institute of Atomic Energy, Beijing 102413, China*

[3]*College of Physics Science and Technology, Shenzhen University, Shenzhen 518060, China*

[4]*Instituto de Física, Universidade Federal Fluminense, Avenida Litoranea s/n, Gragoatá, Niterói, Rio de Janeiro 24210-340, Brazil*

[5]*College of Physics, Jilin University, Changchun 130012, China*

(Received 6 May 2015; published 14 July 2015)

Measurements of complete and incomplete fusion cross sections for ^{6}Li+ ^{154}Sm have been performed at energies above the Coulomb barrier by the online γ-ray method, to investigate the effect of breakup and inelastic couplings on the complete fusion (CF) of this weakly bound system. We show that inelastic excitation couplings have non-negligible effects, when compared with the breakup effect, for deformed nuclei at energies very close to the Coulomb barrier. The average CF suppression corresponding to dynamic breakup effects was found to be around 35%. The total fusion cross section is not affected by the breakup coupling. A comparison between the ^{6}Li-induced CF suppression for three different samarium isotopes shows that the breakup effect is larger for the more spherical isotope.

DOI: 10.1103/PhysRevC.92.014615 PACS number(s): 25.60.Pj, 25.60.Gc, 25.70.Gh, 25.70.Mn

I. INTRODUCTION

Samarium isotopes have been used in the investigation of fusion between heavy ions for a long time. The reason is that there are several stable samarium isotopes, ranging from the almost spherical ^{144}Sm to ^{154}Sm, which has a large static deformation. Odd stable isotopes also exist. The main topic investigated since the late 1970s is the influence of deformation in the sub-barrier fusion reactions. The pioneer work in this field was done by Stokstad *et al.* [1,2], on the sub-barrier fusion of the double-magic ^{16}O with ^{144,148,150,152,154}Sm. Some years later, di Gregorio *et al.* [3,4], also in collaboration with Stokstad, complemented those investigations by measuring sub-barrier fusion with ^{144,147,149}Sm. Some of those systems were measured in the 1990s by the Australian group of Leigh *et al.* [5], in much more precise experiments, where fusion barrier distributions were also derived. Reisdorf *et al.* [6] measured fusion of ^{40}Ar + ^{144,148,154}Sm, and Gil *et al.* [7] and Gomes *et al.* [8] measured fusion of ^{28}Si, ^{32}S + ^{154}Sm, respectively. More recently, fusion and quasifission of ^{40,48}Ca + ^{144,154}Sm were also measured [9,10]. From all those works and from others using different systems, it became very well demonstrated that couplings to inelastic channels enhance the fusion cross section at sub-barrier energies and that nuclei with large deformations, corresponding to very strong couplings to very low-lying excited states, present huge enhancements at this energy regime, compared with predictions from one-dimensional barrier penetration models (1DBPM). As the deformation increases, so does the enhancement. Maciel *et al.* [11] showed that transfer couplings do not affect the sub-barrier fusion of ^{16}O with even Sm isotopes.

In most of the early works on sub-barrier fusion of Sm isotopes, the theory used to be compared with the data was very simple. The most used model was the Wong model [12], which has four free parameters: V_B, R_B, $\hbar w$, and β_2, where V_B is the height of the Coulomb barrier, R_B is its radius, $\hbar w$ is related to the barrier curvature (larger $\hbar w$ means thinner barrier), and β_2 is the quadrupole deformation of the nuclei. V_B and R_B were usually obtained by fitting the fusion data above the barrier and using semiclassical models. This procedure was based on the assumption that at energies above the barrier, there is no coupling-channel effect on the fusion cross section. Then, the other two parameters, $\hbar w$ and β_2, were derived by fitting the sub-barrier energy fusion data. Alternatively, the barrier parameters were derived from proximity potentials and very simplified coupled-channel calculations were used to analyze the sub-barrier energy data.

In recent years, fusion of weakly bound nuclei, both stable and radioactive, was intensively investigated [13], both experimentally and theoretically. The influence of the breakup of those nuclei on the fusion cross section was the main topic under study. Almost all targets used in the experiments were spherical or not very deformed. One of the main reasons for that was to avoid the investigation of a possible breakup effect in systems where the deformation effect on fusion might be much more important than the one under investigation, what could hide breakup effects, at least at sub-barrier energies. From the tens of published works and systems measured, systematic results could be obtained [14–19]. In all those works, fusion cross-sectional data were compared with theoretical predictions that do not take into account breakup and transfer couplings. Of course, if the theoretical calculations for fusion cross sections were complete, including couplings to all possible reaction channels, there should be no difference between their results and the data. However, such kinds of calculations are not available when weakly bound nuclei,

*zgl@buaa.edu.cn
†huan@ciae.ac.cn

and consequently the breakup process, are involved. Even the most sophisticated continuum discretized coupled-channel calculations (CDCC) are not so complete. On the other hand, it is very useful and interesting to perform calculations that leave out some parameters, because in this way the differences between calculated fusion cross sections and the data can be attributed to those missing ingredients. This is the main reason why in most (or all) of the reported works involving the search of systematic effects of the breakup process on the fusion cross section, breakup couplings are not included in the calculations. They can predict only the fusion cross section in the absence of the breakup channel, or the total fusion cross section for the systems under investigation. As in most works, transfer channels are also not included in the calculations; the difference with the data is attributed to the combined effect of breakup plus transfer channels on the total fusion cross section.

Basically, the systematics shows some enhancement of the fusion cross section at sub-barrier energies and a new phenomenon, that is, the suppression of the complete fusion (CF) at energies slightly above the Coulomb barrier, when compared with coupled-channel calculations that do not include breakup and transfer channels. The amount of suppression seems to be independent of the target nuclei (so far, only medium and heavy target nuclei had complete fusion measured), but rather depends on the breakup threshold energy of the weakly bound projectile. This suppression ranges from about 20% to 40% for most of the systems involving the stable weakly bound nuclei ^{6,7}Li and ^{9}Be. The exact suppression factor may also vary in different works, depending on the bare potential used in the calculations. Of course, one cannot use fusion data above the barrier to derive the barrier parameters, as was used in the past; otherwise any effect above the barrier would be vanished out.

In a recent work by Wang *et al.* [17], no couplings to inelastic channels were considered in the calculations for the investigation of the fusion suppression above the barrier, because it was assumed that there were no inelastic coupling effects at this energy regime. Indeed, the systematics obtained for the fusion suppression were similar to those obtained in specific works when these couplings were taken into account. The suppression of fusion at energies near and above the barrier is attributed to breakup couplings because the breakup process produces repulsive polarization potentials [20–25], contrary to what happens in couplings to inelastic and transfer channels, where attractive polarization potentials are produced. When the fusion of one of the projectile fragments (produced by the projectile breakup), named incomplete fusion (ICF), is added to the complete fusion (CF), the total fusion (TF) obtained seems to be not affected by the breakup [13–16,26–28], since the data for all those systems agree with theoretical calculations that do not take into account the breakup couplings.

Concerning fusion of stable weakly bound projectile with samarium isotopes, there are two very interesting papers by Rath *et al.* [29,30] on ^{6}Li + ^{144,152}Sm, at energies below and above the barrier. The sub-barrier energy region was the main concern of the authors, and it was verified that the enhancement for the deformed ^{152}Sm isotope is much stronger than for the vibrational-spherical ^{144}Sm. The main reason, as expected, is the large deformation of ^{152}Sm. At energies above the barrier, both systems show similar fusion suppression. The same conclusion was reached by Wang *et al.* [17] within the systematics for several ^{6}Li-induced fusion with different targets, at energies above the barrier.

Since the fusion suppression above the barrier is not very large, from around 20% to 40%, we decided to investigate also the possible influence of inelastic couplings on fusion at this energy regime, in addition to the breakup effect. We performed experiments to measure fusion cross sections for the ^{6}Li + ^{154}Sm system at energies close to and above the barrier. These data are reported in the present work. The data for ^{6}Li + ^{144,152}Sm at energies above the barrier, previously reported by Rath *et al.* [29,30], are also used in the comparison of data with theory. We also try to disentangle the inelastic and breakup channel effects on the fusion for those spherical and deformed systems by enlarging the comparison of data with calculations at energies slightly above the barrier.

In Sec. II we present the theoretical comparison of coupled-channel calculations including inelastic excitations of the ^{144}Sm and ^{154}Sm targets with one-channel (no-coupling) calculations. In Sec. III we show the experimental setup and details of the experiment. In Sec. IV we present the derivation of fusion cross sections and the results obtained. In Sec. V we discuss the results and make comparison with theoretical predictions. In Sec. VI we compare the breakup effect for fusion of three samarium isotopes by using some previously published data. Finally, in Sec. VII we summarize and present some conclusions.

II. INELASTIC COUPLING EFFECTS AT ENERGIES SLIGHTLY ABOVE THE BARRIER

Before starting the description of the experiment and comparison of fusion data with theoretical predictions, we report the theoretical investigation of possible effects of inelastic coupling on the ^{6}Li fusion cross section at energies slightly above the Coulomb barrier, for the spherical-vibrational ^{144}Sm and well-deformed ^{154}Sm targets. As mentioned in the introduction section, although this effect is supposed to be negligible, we were curious about a possible nonvanishing effect not much smaller than the breakup effect on fusion at this energy region.

The calculations were performed using the double-folding Sao Paulo potential [31,32], which has been successfully used in recent years. Alternatively, the Akyü-Winther potential [33], an approximation of double-folding potential with an analytical form, could also be used, leading to similar results. Both potentials have no free parameters [34]. The code FRESCO [35] was used in the calculations. The no-coupling (one-channel) results are shown in Figs. 1(a) and 2(a) by the full curves for the ^{144}Sm and ^{154}Sm, respectively. The vertical arrows show the positions of the Coulomb barriers. The figures show energies from slightly below to slightly above the barrier, our region of interest.

For the coupled-channel calculations, the following excitations were considered: for ^{144}Sm, the 2^{+} (1660 keV) and 3^{-} (1810 keV) states, with $\beta_2 = 0.087$ [36] and $\beta_3 = 0.15$

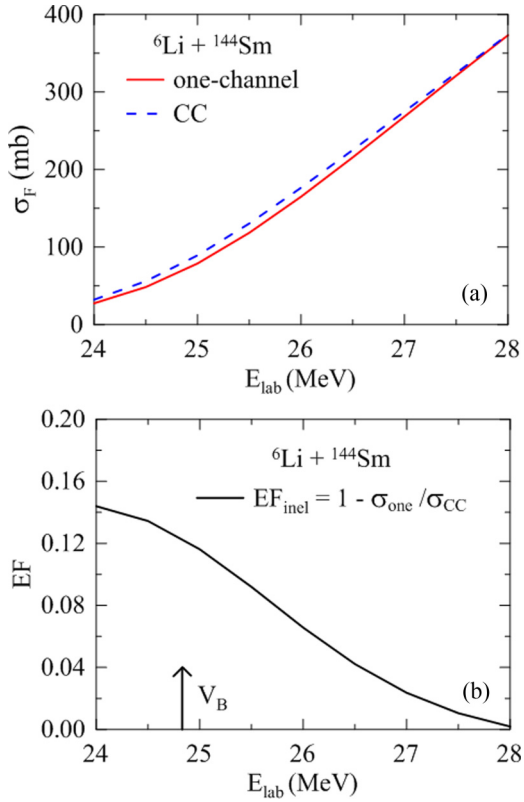

FIG. 1. (Color online) The calculation results of ^{6}Li+ ^{144}Sm system. (a) One-channel and coupling channel (CC). (b) The quantity EF_{inel} as a function of energy; see text for details.

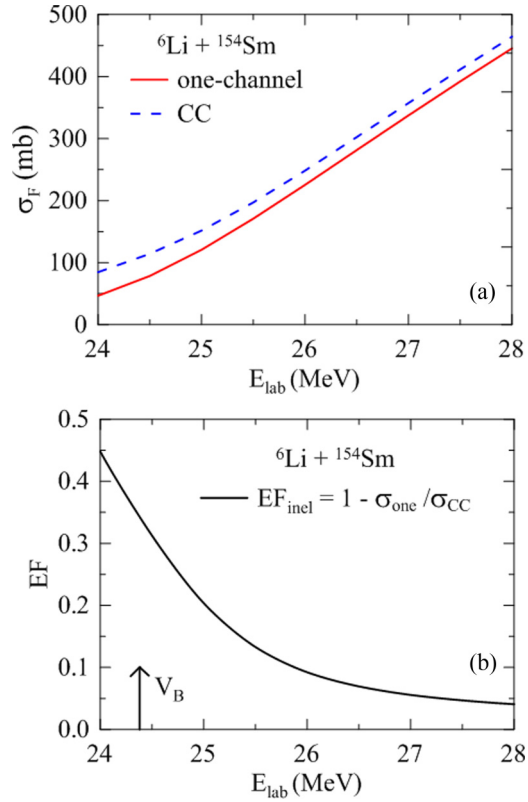

FIG. 2. (Color online) The calculation results of ^{6}Li+ ^{154}Sm. (a) One-channel and coupling channel (CC). (b) The quantity EF_{inel} as a function of energy; see text for details.

[37], and for the deformed ^{154}Sm, the 2^+ (82 keV) and 4^+ (267 keV) states, with $\beta_2 = 0.341$ [36] and $\beta_4 = 0.08$ [5]. No couplings corresponding to the ^{6}Li projectile were included, since it has no bound state and its resonances are already connected to breakup couplings. The results are shown by the dashed curves in Figs. 1(a) and 2(a). One can observe that the effect is really negligible for the ^{144}Sm, but not so much for the deformed ^{154}Sm, for which the effect at sub-barrier energies is much more important than for the ^{144}Sm isotope. The coupled-channel calculations are above the one-channel calculations. The effects can be more clearly identified when one plots the quantity $EF_{inel} = 1 - \sigma_{one}/\sigma_{CC}$, as shown in Figs. 1(b) and 2(b). For the ^{144}Sm, the enhancement due to inelastic couplings is 12% at the barrier and drops to 1% at $1.13V_B$, whereas for the ^{154}Sm, the enhancement is 30% at the barrier and 5% at $1.13V_B$. Since this is the energy region of most interest when one is investigating breakup effects on fusion, which is of the order of 20% to 40%, we observe that inelastic couplings should not be neglected, at least when one is dealing with highly deformed targets.

III. EXPERIMENTAL DETAILS

The experiment was carried out with a $^{6}Li^{3+}$ beam at the HI-13 Tandem Accelerator of China Institute of Atomic Energy (CIAE) in Beijing at bombarding energies from 26 to 36 MeV in steps of 2 MeV. The nominal Coulomb barrier is ~24.9 MeV at the laboratory frame (~24.0 MeV in the c.m. frame). A 99% enriched ^{154}Sm metallic foil with 1.98 mg/cm^2 thickness was used. The fusion excitation function was measured using the online characteristic γ spectrometry method. The irradiation times lasted 1–2 h at all energies for the single γ-ray measurements. The beam current was varied from 1.9 to 5.0 pnA, and the beam flux was recorded by a Faraday cup mounted behind the target using a precise current integrator device. Two Si(Au) surface barrier detectors were positioned at 30° with respect to the beam direction for verification of the beam intensity, normalization, and centrality of the beam. An array consisting of nine Compton-suppressed BGO-HPGe spectrometers and two planar HPGe detectors was used to detect online γ rays emitted by the reaction products. The absolute efficiency and energy calibration of the detectors were achieved using a set of standard radioactive sources of ^{152}Eu and ^{133}Ba at the target position. The Versa Module Europa (VME)–based data acquisition system MIDAS was used to record the data. The total uncertainty in this experiment mainly came from the statistical errors associated with the yields of the γ rays and from the systematic errors in the target thickness as well as the estimation of the beam intensity. The typical characteristic γ spectrum for the ^{6}Li+ ^{154}Sm fusion system at $E_{lab} = 32$ MeV is given in Fig. 3, where several identified channels via complete and incomplete fusions are denoted.

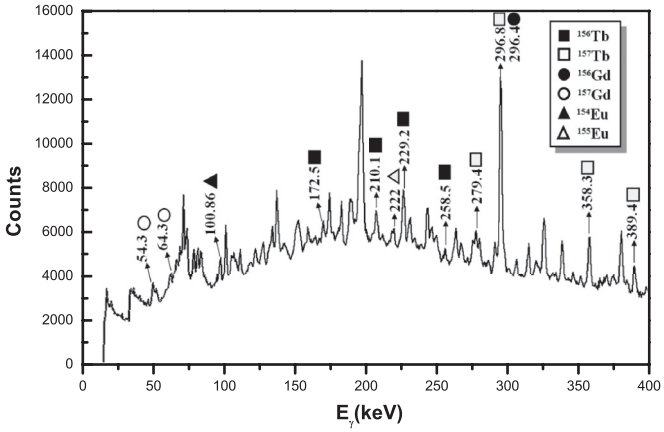

FIG. 3. Typical online γ-ray spectrum depicting the γ lines of different evaporation residues via complete and incomplete fusions in the ^{6}Li+ ^{154}Sm system at the bombarding energy of 32 MeV.

IV. DERIVATION OF FUSION CROSS SECTIONS

The compound nucleus formed following the collision of ^{6}Li and ^{154}Sm is ^{160}Tb, which then decays predominantly by neutron evaporation, leading to different Tb isotopes. The dominant decay channels are observed to be $3n$ and $4n$ evaporations at all energies, which agree well with a statistical model calculation using the code PACE2 [38]. The transitions feeding the residue nuclei of CF, given in Table I, were identified and used in the calculations.

The fusion cross section for the online measurement is calculated using the relation

$$\sigma_\gamma = \frac{N_\gamma}{\varepsilon_\gamma N_B N_T}, \tag{1}$$

where ε_γ is the absolute efficiency of all the detectors for the γ lines, N_B and N_T represent the total number of beam particles incident on the target and the target atoms per unit area, respectively, and N_γ denotes the yield of the γ-ray peak after correcting with the internal conversion. The cross sections of individual residues equal to the sum of cross sections of all observed ground-state feeding transitions. It is to be mentioned that the intensities of some transitions were too small to be observed, and thus the fraction of these γ-rays is neglected for the present system.

In order to obtain the relative contribution of other residue channels to CF, the statistical model code PACE2 was used for the calculations. The L distribution obtained from the CCFULL [41] calculations was used as an input of PACE2 at each energy.

TABLE I. Characteristic γ rays of ^{156}Tb [39] and ^{157}Tb [40] used in the CF calculation.

Residual channels	Transitions	E_γ (keV)	I_γ (%)
^{156}Tb(4n)	$16^- \longrightarrow 15^-$	229.2	165
^{157}Tb(3n)	$7/2^- \longrightarrow 5/2^+$	296.8	190

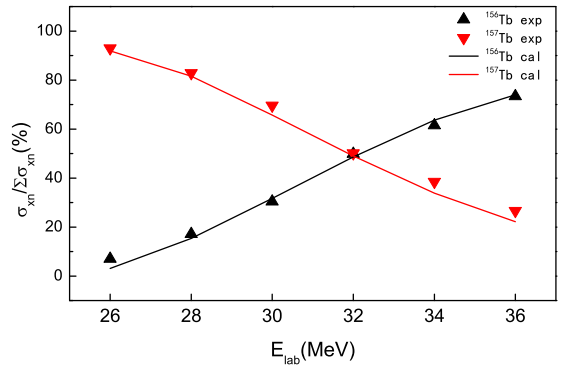

FIG. 4. (Color online) Ratio of individual channel cross sections to the CF cross sections as a function of beam energy for ^{6}Li+ ^{154}Sm. The solid lines represent the theoretical estimation of PACE2.

$R_\delta^{\text{theory}} = \Sigma_x \delta_{xn}^{\text{PACE2}}/\delta_{\text{fus}}^{\text{PACE2}}$ $(x = 3,4)$ was calculated and the results indicate that the summed cross sections of $3n$ and $4n$ channels contribute from 95.1% to 97.6% of the complete fusion cross section for the ^{6}Li+ ^{154}Sm system. Figure 4 shows the individual xn channel cross sections normalized to the CF cross sections for the reaction ^{6}Li+ ^{154}Sm. A reasonable agreement between the $\delta_{xn}^{\text{Pace}}$ and measured $\delta_{xn}^{\text{Exp.}}$ is observed over the whole energy range. As can be observed in Table II, the contributions of other evaporation residues to the total complete fusion are small and the total complete fusion cross section was derived by $\sigma_{\text{fus}}^{\text{exp}} = \Sigma\sigma_{xn}^{\text{exp}}/R_\delta^{\text{theory}}$.

A similar procedure was used to derive the ICF cross sections. Although the main aim of this work is the measurement of CF cross section, our experimental method allows us to also measure the ICF. However, for ICF we could only determine the lower limits for the cross sections, because some γ lines corresponding to some evaporation channels were too weak above the background to be used for the cross-section determination. Table III shows the characteristic γ lines used to derive the ICF cross sections. The ^{156}Gd nucleus is produced by neutron evaporation from the compound nucleus formed by absorption of an α particle by the target. The ^{154}Eu nucleus is produced by neutron evaporation from the compound nucleus formed by absorption of a proton or deuteron by the target.

Table IV shows the cross sections for each of those evaporation channels. Table V shows the CF and the lower limits of ICF and TF for the ^{6}Li + ^{154}Sm system. Figure 5 shows the experimental excitation functions obtained of CF

TABLE II. The cross sections for $3n$-ER, $4n$-ER and total complete fusion with R_δ^{theory} obtained from PACE2 calculations.

E_{lab} (MeV)	$E_{\text{c.m.}}$ (MeV)	$\sigma_{3n+4n}^{\text{Exp.}}$ (mb)	R_δ^{theory} (%)	$\sigma_{\text{fus}}^{\text{exp}}$ (mb)
36.0	34.6	718.25 ± 37.83	96.2%	746.62 ± 39.32
34.0	32.7	646.04 ± 28.90	97.5%	662.61 ± 29.64
32.0	30.8	496.49 ± 22.91	97.6%	508.70 ± 23.48
30.0	28.9	409.53 ± 18.19	97.4%	420.46 ± 18.68
28.0	27.0	247.39 ± 13.03	97.0%	255.04 ± 13.43
26.0	25.0	112.10 ± 7.19	95.1%	117.88 ± 7.56

TABLE III. Characteristic γ rays of ^{156}Gd [42] and ^{154}Eu [43] used in the ICF calculation.

Residual channels	Transitions	E_γ (keV)	I_γ
^{156}Gd	$6^+ \longrightarrow 4^+$	296.4	100%
^{154}Eu	$4^+ \longrightarrow 3^-$	100.86	713.3[a]

[a]This value denotes the γ intensity per 10^4 neutron [43].

and the lower limits of ICF and TF in the present work, for the ^{6}Li+ ^{154}Sm system. ICF and TF correspond actually to the lower limits of the cross sections, as explained before. The not very smooth behavior of the ICF excitation function is due to the relative larger fraction of the cross section corresponding to the nonmeasured γ lines, which were more important at midenergies.

V. DISCUSSION OF THE COUPLING EFFECTS ON THE FUSION CROSS SECTION

In this section we compare the CF and lower limit of the TF cross sections with theoretical predictions, including or not the couplings to inelastic channels of the ^{154}Sm target. It is important to mention again that in our calculations there are no free parameters, in a such way that their results are theoretical predictions rather than any kind of fit. The potential used was the double-folding Sao Paulo potential [31,32] and the description of the inelastic excitation couplings was already presented in Sec. II. We use linear scale plots, in order to observe the effects at energies above the barrier better than if we had used logarithmic scale, which is more suitable for the investigation of effects at sub-barrier energies. It is important to mention again that in the calculations, the breakup and transfer couplings were not taken into account. In this way, the difference between the experimental fusion cross sections (CF or TF) and the calculations is originated either by combined effects of breakup plus transfer plus inelastic excitations of the projectile or just the breakup plus transfer couplings, the latter corresponding to the calculations in which the inelastic excitations of the target nucleus was included in the coupled channel scheme.

Figure 6 shows the measured data for CF and the lower limit for the TF, in comparison with the predictions, including the couplings of inelastic excitations of the ^{154}Sm. One can observe that the TF cross section is almost in agreement with the calculations. Actually, it is slightly below the calculations, which can be explained by the lack of the measurement of all γ-ray transitions corresponding to ICF, as already mentioned in Sec. IV. However, the results show that the missing contribution to ICF is very small. The behavior of the TF excitation function is in agreement with what was observed in several published papers [13–16,26–28]; that is, there is no effect of breakup couplings on the TF cross sections, which means there is no effect of breakup plus transfer couplings on the TF cross sections, since those are the channels not included in the coupled channel calculations. Since the transfer coupling at energies above the barrier is usually considered to be negligible, this means that the suppression of CF at energies above the barrier is attributed to the loss of flux from the elastic channel to the ICF process, which otherwise would go to CF.

Concerning the CF excitation function, Fig. 6 shows that there is an average suppression of the order of 35%, compatible with the suppression found for several other systems including stable weakly bound projectiles [14–19].

In Fig. 7 we plot the CF suppression factor as a function of the center-of-mass energy divided by the Coulomb barrier energy. We show two quantities:

$SF_{\rm one} = 1 - \frac{\sigma_{\rm exp}^{\rm CF}}{\sigma_{\rm one}^{\rm TF}}$ and $SF_{\rm CC} = 1 - \frac{\sigma_{\rm exp}^{\rm CF}}{\sigma_{\rm CC}^{\rm TF}}$. $SF_{\rm one}$ corresponds to the CF suppression in relation to calculations that do not take into account any couplings. So, this suppression corresponds to the overall coupling channels, including inelastic excitations of the target, transfer couplings, and breakup couplings. $SF_{\rm CC}$

TABLE IV. The lower limits of cross sections for each of ICF evaporation channels of ^{6}Li+ ^{154}Sm system.

$E_{\rm lab}$ (MeV)	σ_f (^{156}Gd) (mb)	σ_f (^{154}Eu) (mb)
36.0	138.8 ± 3.23	170.03 ± 36.70
34.0	88.23 ± 2.02	175.17 ± 25.57
32.0	74.07 ± 1.91	181.71 ± 25.65
30.0	33.09 ± 1.45	146.55 ± 16.80
28.0	31.90 ± 1.94	111.77 ± 56.09
26.0	0	88.30 ± 88.30

TABLE V. The cross sections of CF and lower limits of cross sections of ICF and TF for ^{6}Li+ ^{154}Sm system.

$E_{\rm lab}$ (MeV)	$\sigma_{\rm CF}$ (mb)	$\sigma_{\rm ICF}$ (mb)	$\sigma_{\rm TF}$ (mb)
36.0	746.62 ± 39.32	308.90 ± 36.84	1055.5 ± 53.88
34.0	662.61 ± 29.64	263.40 ± 25.65	926.01 ± 39.20
32.0	508.70 ± 23.48	255.78 ± 25.72	764.48 ± 34.83
30.0	420.46 ± 18.68	179.64 ± 16.86	600.10 ± 25.16
28.0	255.04 ± 13.43	143.67 ± 56.12	398.71 ± 57.70
26.0	117.88 ± 7.56	88.30 ± 88.30	206.18 ± 88.62

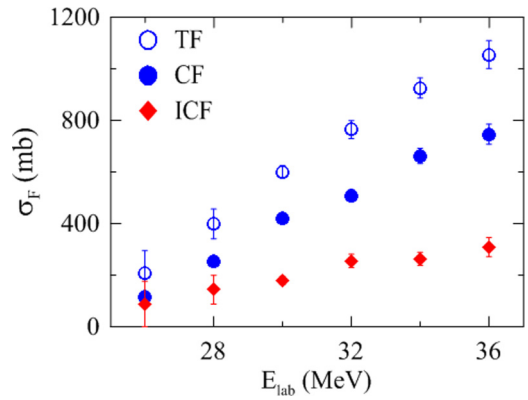

FIG. 5. (Color online) Measured complete, incomplete, and total fusion cross sections at energies above the Coulomb barrier.

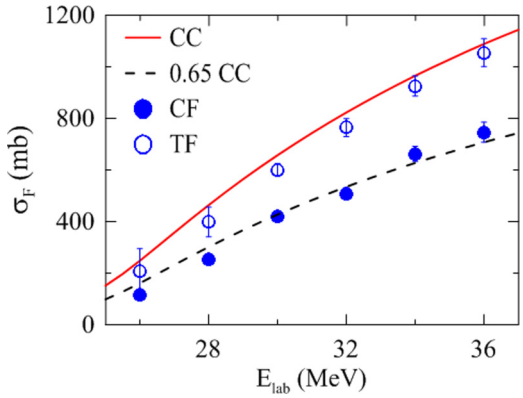

FIG. 6. (Color online) Measured complete and lower limit of total fusion cross sections. The full curve is the result of coupling-channel calculations including the target excited states. The dashed curve is the same full curve multiplied by 0.65, corresponding to an average CF suppression factor of 35%.

corresponds to the CF suppression in relation to calculations that take into account the inelastic excitation couplings. So, this suppression corresponds to the coupling of channels not included in the calculations, that is, transfer and breakup couplings. From now on, we will assume that this effect is attributed only to breakup couplings, although possible transfer coupling effects are included in it.

One can observe that, in agreement with what was shown in Fig. 2, the inelastic couplings are not negligible at energies very close to the Coulomb barrier. For the energies of $V_B/E_{\text{c.m.}}$ up to 1.2, a smaller suppression factor is observed in relation to the no-coupling calculations than with the calculations that consider inelastic couplings. This is explained by the enhancement in the CF cross section produced by inelastic excitations of the deformed target at energies close but above the barrier. In Sec. II we have shown that this effect is negligible for the spherical-vibrational ^{144}Sm target. The reason for this enhancement may be understood by the attractive polarization

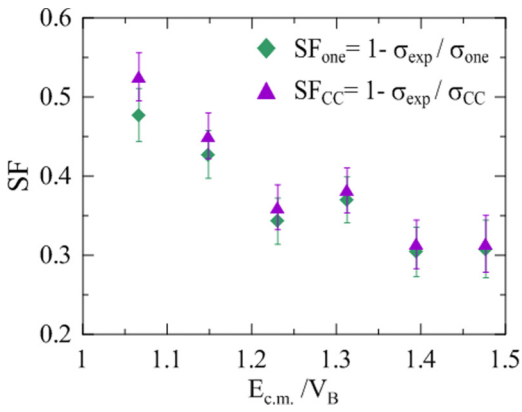

FIG. 7. (Color online) Complete fusion suppression factor as a function of energy. The diamonds (green online) are the suppression when compared with one-channel calculations, whereas the triangles (purple online) are the suppression compared with coupling-channel calculations including the target excited states.

potential produced by the inelastic excitations, which is much more intense for low-lying excitations (deformed nuclei) than for higher excitations. On the contrary, the breakup produces repulsive polarization potential and this potential is larger at energies close to the barrier than when the energy increases, as demonstrated in several published works on breakup threshold anomaly [44,45] in the elastic scattering of weakly bound nuclei. When the energy increases, the breakup polarization potential becomes approximately constant. One can observe a consequence of this behavior by the decrease of the CF suppression factor as the energy increases, shown in Fig. 7, and becoming roughly constant at larger energies. Similar behavior of the energy dependence of the CF suppression factors at energies above the barrier was shown for other weakly bound systems in previously reported works [26–28,46].

VI. COMPARISON OF THE BREAKUP COUPLING EFFECT ON CF CROSS SECTIONS FOR DIFFERENT SAMARIUM ISOTOPES

In this section we compare the effects of breakup couplings (named dynamical effects) on the CF of three samarium isotopes. The data for the ^{6}Li + ^{144}Sm and ^{152}Sm are from Rath *et al.* [29,30]. Of course, when one wants to compare different systems in the same plot, some reduction procedure has to be performed, to wash out static effects such as different sizes and charges or specific properties related with possible diffuse densities of some nuclei.

Canto *et al.* [15] have shown that the reduction method that fully eliminates all the static effects is the one that plots two dimensionless quantities. In the vertical axis one plots $F(x) = (2E_{\text{c.m.}}/\pi R_B^2 \hbar\omega)\sigma_{\text{fus}}$, where V_B, R_B, and $\hbar w$ are the barrier height, radius, and the curvature of the Coulomb barrier, respectively. In the horizontal axis one uses the energy variable x, defined as $x = (E_{\text{c.m.}} - V_B)/\hbar w$. A benchmark curve written as $F_0(x) = \ln[1 + \exp(2\pi x)]$ is called universal fusion function (UFF). This method is inspired by the simple Wong model [12]. If the Wong model is valid and no coupling effect on the fusion cross section is present, the experimental fusion function coincides with the UFF curve. A renormalization of the experimental fusion function has to be made to take into account the possible failure of the Wong model (it is not valid for light systems at sub-barrier energies) and effects of some coupling channels [15]. Then the renormalized experimental fusion function becomes $\bar{F}_{\text{exp}} = F_{\text{exp}} \frac{F_0(x)}{F_{\text{CC}}(x)}$, where F_{CC}(x) is the fusion cross sections calculated by a more realistic potential and taking into account some coupling channels. When this renormalization of the data is performed, the difference between the UFF curve and the renormalized experimental fusion function corresponds to the coupling (dynamical) effects of the channels not included in the coupling-channel calculations.

In the present work, breakup and transfer channels were not included in the coupled-channel calculations. The inelastic excitation couplings for the ^{144}Sm and ^{154}Sm were already described in Sec. II. For ^{152}Sm, the 2^+ (121.8 keV) and 4^+ (366.5 keV) states with $\beta_2 = 0.306$ [36] were considered.

The results are shown in Fig. 8. One can observe that the CF suppressions for the three systems are similar at energies very

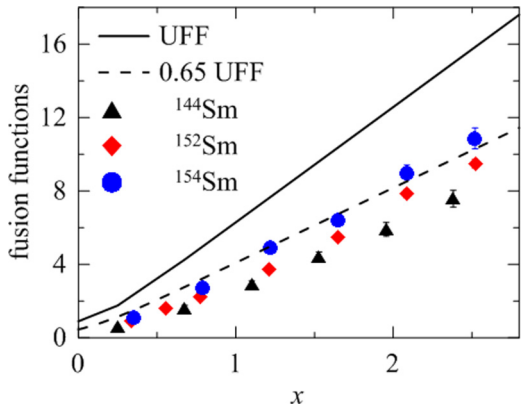

FIG. 8. (Color online) Renormalized experimental fusion functions for the CF of ^{6}Li with three Sm isotopes. The full curve is the UFF. The suppression in relation to the UFF curve is attributed to dynamical effects due to breakup. See text for details.

close to the Coulomb barrier, but when the energy increases, the vibrational ^{144}Sm isotope presents a larger suppression than the deformed ^{152}Sm, and the smallest suppression is found for the most deformed ^{154}Sm. Once again, it is important to mention that we have already taken into account the fact that as the mass A is larger, the size of the system is larger. So, the effect shown in Fig. 8 is due to dynamic effects. The reason for this behavior has to be further investigated both theoretically and also by the measurement of fusion of other systems for which there are almost spherical and deformed isotopes, like Sm, or even to measure CF of Sm isotopes with other stable weakly bound nuclei.

VII. SUMMARY

We report the measurement of complete fusion (CF) cross sections for ^{6}Li+ ^{154}Sm system at energies above the Coulomb barrier. The method used was the online γ-ray method, which allowed the measurement of almost 100% of the CF. Furthermore, we measured the lower limit of incomplete fusion cross sections, because some of the γ-ray lines could not be measured.

We investigated the effect of breakup and inelastic couplings on the CF cross section at energies above the Coulomb barrier. We have shown that inelastic excitation couplings have non-negligible effects, when compared with the breakup effect, for deformed nuclei at energies up to 20% above the Coulomb barrier. The CF suppression decreases when the energy increases above the barrier and reaches a constant average value of 35% from energies of the order of 30% above the barrier. These results are similar to the ones found for other weakly bound systems. We interpret that this breakup effect corresponds to the repulsive polarization potential produced by the breakup, which is larger at the barrier energy. The TF cross section is not affected by the breakup coupling. A comparison between the ^{6}Li-induced CF suppression for three different samarium isotopes shows that the breakup effect (suppression) is larger for the more spherical isotope. This is a very interesting result that deserves further theoretical and experimental investigations.

ACKNOWLEDGMENTS

This work is supported by National Natural Science Foundation of China under Grants No. 11475013, No. 11035007, No. 11175011, No. 11375266, No. 11375267, No. 11305269, No. 11175259, No. 11475072, No. 11405274, and No. 10775098 and State Key Laboratory of Software Development Environment (SKLSDE-2014ZX-08), as well as by the Fundamental Research Funds for the Central Universities and the Key Laboratory of High Precision Nuclear Spectroscopy, Institute of Modern Physics, Chinese Academy of Sciences. This work also benefited from discussions held at the CUSTIPEN. P. R. S. Gomes and J. Lubian thank the CNPq, CAPES, and FAPERJ for their financial support. The authors thank the crew of the HI-13 tandem accelerator at the China Institute of Atomic Energy for steady operation of the accelerator. We are also grateful to Q. W. Fan for preparing the target.

[1] R. G. Stokstad, Y. Eisen, S. Kaplanis, D. Pelte, U. Smilansky, and I. Tserruya, Phys. Rev. Lett. **41**, 465 (1978).
[2] R. G. Stokstad, Y. Eisen, S. Kaplanis, D. Pelte, U. Smilansky, and I. Tserruya, Phys. Rev. C **21**, 2427 (1980).
[3] D. E. Di Gregorio *et al.*, Phys. Lett. B **176**, 322 (1986).
[4] D. E. Di Gregorio *et al.*, Phys. Rev. C **39**, 516 (1989).
[5] J. R. Leigh *et al.*, Phys. Rev. C **52**, 3151 (1995).
[6] W. Reisdorf *et al.*, Nucl. Phys. A **438**, 212 (1985).
[7] S. Gil *et al.*, Phys. Rev. Lett. **65**, 3100 (1990).
[8] P. R. S. Gomes *et al.*, Phys. Rev. C **49**, 245 (1994).
[9] G. N. Knyazheva *et al.*, Phys. Rev. C **75**, 064602 (2007).
[10] A. M. Stefanini *et al.*, Eur. Phys. J. A **23**, 473 (2005).
[11] A. M. M. Maciel and P. R. S. Gomes, Phys. Rev. C **53**, 1981 (1996).
[12] C. Y. Wong, Phys. Rev. Lett. **31**, 766 (1973).
[13] L. F. Canto, P. R. S. Gomes, R. Donangelo, and M. S. Hussein, Phys. Rep. **424**, 1 (2006).
[14] L. F. Canto, P. R. S. Gomes, J. Lubian, L. C. Chamon, and E. Crema, Nucl. Phys. A **821**, 51 (2009).
[15] L. F. Canto, P. R. S. Gomes, J. Lubian, L. C. Chamon, and E. Crema, J. Phys. G **36**, 015109 (2009).
[16] P. R. S. Gomes, J. Lubian, and L. F. Canto, Phys. Rev. C **79**, 027606 (2009).
[17] B. Wang, W. J. Zhao, P. R. S. Gomes, E. G. Zhao, and S. G. Zhou, Phys. Rev. C **90**, 034612 (2014).
[18] P. R. S. Gomes, L. F. Canto, J. Lubian, and M. S. Hussein, Phys. Lett. B **695**, 320 (2011).
[19] P. R. S. Gomes, R. Linares, J. Lubian, C. C. Lopes, E. N. Cardozo, B. H. F. Pereira, and I. Padron, Phys. Rev. C **84**, 014615 (2011).
[20] N. Keeley, N. Alamanos, K. Rusek, and K. W. Kemper, Phys. Rev. C **71**, 014611 (2005).
[21] S. Santra, S. Kailas, K. Ramachandran, V. V. Parkar, V. Jha, B. J. Roy, and P. Shukla, Phys. Rev. C **83**, 034616 (2011).

[22] J. Lubian *et al.*, Nucl. Phys. A **791**, 24 (2007).
[23] J. Lubian, T. Correa, P. R. S. Gomes, and L. F. Canto, Phys. Rev. C **78**, 064615 (2008).
[24] J. Lubian, T. Correa, E. F. Aguilera, L. F. Canto, A. Gomez-Camacho, E. M. Quiroz, and P. R. S. Gomes, Phys. Rev. C **79**, 064605 (2009).
[25] V. V. Parkar, V. Jha, S. K. Pandit, S. Santra, and S. Kailas, Phys. Rev. C **87**, 034602 (2013).
[26] M. Dasgupta *et al.*, Phys. Rev. Lett. **82**, 1395 (1999).
[27] M. Dasgupta *et al.*, Phys. Rev. C **70**, 024606 (2004).
[28] S. Kumar and Y. G. Ma, Phys. Rev. C **91**, 034612 (2015).
[29] P. K. Rath *et al.*, Phys. Rev. C **79**, R051601 (2009).
[30] P. K. Rath *et al.*, Nucl. Phys. A **874**, 14 (2012).
[31] L. C. Chamon, D. Pereira, M. S. Hussein, M. A. Cándido Ribeiro, and D. Galetti, Phys. Rev. Lett. **79**, 5218 (1997).
[32] L. C. Chamon *et al.*, Phys. Rev. C **66**, 014610 (2002).
[33] O. Akyuz and A. Winther, in *Nuclear Structure of Heavy Ion Reactions*, edited by R. A. Broglia, C. H. Dasso, and R. A. Ricci (North Holland).
[34] L. F. Canto, P. R. S. Gomes, J. Lubian, M. S. Hussein, and P. Lotti, Eur. Phys. J. A **50**, 89 (2014).
[35] I. J. Thompson, Comp. Phys. Rev. Rep. **7**, 167 (1988).
[36] S. Raman, C. W. Nestor Jr., and P. Tikkanem, At. Data Nucl. Data Tables **78**, 1 (2001).
[37] T. Kibedi and R. H. Spear, At. Data Nucl. Data Tables **80**, 35 (2001).
[38] A. Gavron, Phys. Rev. C **21**, 230 (1980).
[39] R. Bengtsson *et al.*, Nucl. Phys. A **389**, 158 (1982).
[40] D. J. Hartley *et al.*, Phys. Rev. C **57**, 2944 (1998).
[41] K. Hagino, N. Rowley, and A. T. Kruppa, Comp. Phys. Commun. **123**, 143 (1999).
[42] M. Sagawara *et al.*, Nucl. Phys. A **686**, 29 (2001).
[43] W. Stö, D. Rabenstein, K. Schreckenbach, and T. von Egidy, Z. Phys. A **282**, 97 (1977).
[44] M. S. Hussein, P. R. S. Gomes, J. Lubian, and L. C. Chamon, Phys. Rev. C **73**, 044610 (2006).
[45] M. S. Hussein, P. R. S. Gomes, J. Lubian, and L. C. Chamon, Phys. Rev. C **76**, 019902(E) (2007).
[46] N. T. Zhang *et al.*, Phys. Rev. C **90**, 024621 (2014).